◆ Human Brain Mapping 29:329–345 (2008) ◆

Noncanonical Spike-Related BOLD Responses in Focal Epilepsy

Louis Lemieux,[1,2]* Helmut Laufs,[1,2] David Carmichael,[1,2] Joseph Suresh Paul,[1,2] Matthew C. Walker,[1,2] and John S. Duncan[1,2]

[1]*Department of Clinical and Experimental Epilepsy, Institute of Neurology, University College London, Queen Square, London, United Kingdom*
[2]*MRI Unit, National Society for Epilepsy, Chalfont St. Peter, Buckinghamshire, United Kingdom*

Abstract: Till now, most studies of the Blood Oxygen Level-Dependent (BOLD) response to interictal epileptic discharges (IED) have assumed that its time course matches closely to that of brief physiological stimuli, commonly called the canonical event-related haemodynamic response function (canonical HRF). Analyses based on that assumption have produced significant response patterns that are generally concordant with prior electroclinical data. In this work, we used a more flexible model of the event-related response, a Fourier basis set, to investigate the presence of other responses in relation to individual IED in 30 experiments in patients with focal epilepsy. We found significant responses that had a noncanonical time course in 37% of cases, compared with 40% for the conventional, canonical HRF-based approach. In two cases, the Fourier analysis suggested activations where the conventional model did not. The noncanonical activations were almost always remote from the presumed generator of epileptiform activity. In the majority of cases with noncanonical responses, the noncanonical responses in single-voxel clusters were suggestive of artifacts. We did not find evidence for IED-related noncanonical HRFs arising from areas of pathology, suggesting that the BOLD response to IED is primarily canonical. Noncanonical responses may represent a number of phenomena, including artefacts and propagated epileptiform activity. *Hum Brain Mapp 29:329–345, 2008.*

Key words: epilepsy; fMRI; EEG; EEG-fMRI; BOLD; haemodynamic response; localization

INTRODUCTION

EEG-correlated functional MRI (fMRI) can be useful to investigate interictal discharge- (IED) related Blood Oxygen Level-Dependent (BOLD) responses in patients with focal epilepsy [Hamandi et al., 2004; Krakow et al., 1999, 2001; Lazeyras et al., 2000; Lemieux et al., 2001; Patel et al., 1999; Salek-Haddadi et al., 2003; Seeck et al., 1998; Warach et al., 1996]. The haemodynamic response function (HRF) describes the characteristic BOLD response to a brief neural event and thus characterizes the input (neural excitation)–output (deoxy-haemoglobin content in the venous drainage) behavior at any given voxel. The shape of the HRF associated with various stimuli has been shown to vary across the brain regions and from subject to subject

Contract grant sponsor: Medical Research Council; Contract grant number: G0301067; Contract grant sponsor: Wellcome Trust; Contract grant number: G67176; Contract grant sponsor: Deutsche Forschungsgemeinschaft; Contract grant number: LA 1452/3-1

*Correspondence to: Professor Louis Lemieux, MRI Unit, National Society for Epilepsy, Chesham Lane, Chalfont St. Peter, Buckinghamshire SL9 0RJ, United Kingdom.
E-mail: l.lemieux@ion.ucl.ac.uk

Received for publication 17 October 2006; Revised 12 February 2007; Accepted 18 February 2007

DOI: 10.1002/hbm.20389
Published online 17 May 2007 in Wiley InterScience (www.interscience.wiley.com).

[Handwerker et al., 2004], but retains a characteristic shape with a peak response within the first 4–6 s of activation followed by a rebound and decreased signal change for 8–10 s.

The standard modeling approach to event-related fMRI analysis treats each voxel as an independent linear time-invariant system, and requires the specification of the HRF for convolution with the event onsets, in a General Linear Model (GLM) framework [Friston et al., 1995b; Rajapakse et al., 1998]. A large degree of normal variability can be accommodated by the addition of the first temporal derivative (TD) to the canonical HRF [Friston et al., 1998] (HRF+TD approach) (Statistical Parametric Mapping [SPM, http://www.fil.ion.ucl.ac.uk/spm]). Using this approach, we previously demonstrated patterns of positive BOLD changes that were mostly concordant with the presumed source of the IED as inferred from electro-clinical data [Salek-Haddadi et al., 2006]. In addition, significant remote responses corresponding to BOLD increases and decreases were observed. In some cases multiple areas of significant responses were linked to a single IED type, and these areas were often very close to each other and probably represent a single irritative zone [Benar et al., 2002; Lemieux et al., 2001; Seeck et al., 1998]. The occurrence of IED-related BOLD decreases, corresponding to an inverted SPM-canonical response, is less preponderant in focal epilepsy than BOLD increases and with poorer concordance with the presumed IED generators [Bagshaw et al., 2005; Salek-Haddadi et al., 2006]. Using spike-triggered 'burst-mode' fMRI, Krakow et al. found peak BOLD response times in the range 1.5–7.5 s [Krakow et al., 2001].

Analyses based on the canonical HRF reveal plausible activation patterns in cognitive studies on healthy subjects and for IED-related studies in patients with epilepsy, but it has been suggested that the spectrum of haemodynamic responses associated with IED may be broader; possibly reflecting various aspects of the underlying pathology [Benar et al., 2002; Friston et al., 1995a; Salek-Haddadi et al., 2003]. To allow for more interregional variation in HRFs, linear combinations of more general basis functions such as the Fourier set can be used [Friston et al., 1995a]. This approach allows one to address the following questions: at what voxels do the event-related responses have a consistent, but arbitrarily (within the constraints of the chosen basis set) shaped, time course across events; and what is this time-course?

Significant response patterns similar to those obtained using the conventional canonical HRF-based approach have been revealed using Fourier set-based analyses in selected patients with focal IED, with a response time course close to the canonical shape. There were however, additional previously unrevealed responses remote from the presumed primary generator [Diehl et al., 2003; Lemieux et al., 2001; Salek-Haddadi et al., 2003]. This approach has been used to demonstrate preserved neurovascular coupling following cancer treatment [Zou et al., 2005]. Lu et al. compared various modeling strategies in selected patients with focal and generalized epilepsies showing interregional response variability, which may have been amplified due to a limitation of the specific deconvolution method used [Lu et al., 2006]. We used a Fourier set based analysis in a series of patients for whom the canonical HRF model did not reveal significant responses; this resulted in a small increase in yield, with noncanonical responses remote from the presumed generator of the epileptiform discharges [Salek-Haddadi et al., 2006].

To increase our understanding of this phenomenon, we set out to investigate the presence of IED-related responses that deviate from the canonical shape in relation to the presumed generators of the IED in a consecutive series of patients with focal epilepsy. In summary, we analyzed IED-related responses with two, nested, linear models. The canonical model included only the canonical hemodynamic response function and its temporal derivative. The extended model included, in addition, a Fourier set allowing for noncanonical response forms. To test for noncanonical responses we specified an F-contrast matrix testing for an effect that could be explained by the Fourier set regressors. Critically, these tests for responses that can be modeled by the Fourier set and cannot be modeled by the canonical regressors. In other words, a noncanonical response is defined as a significant event-related response having explained away the canonical component. We compared the findings with electro-clinical localization.

METHODS

Patients

Sixty-three patients (25 male) with focal epilepsy were recruited from the epilepsy clinics at the National Hospital for Neurology and Neurosurgery, and the National Society for Epilepsy on the basis of frequent interictal epileptic discharges (IED) (spikes, poly-spikes, and sharp waves) on a previous EEG. The study was approved by the Joint Ethics Committee of the National Hospital for Neurology and Neurosurgery, and Institute of Neurology and all subjects gave informed, written consent. The findings for this group of patients based on the canonical model of the haemodynamic response function (HRF) were the subject of a previous publication [Salek-Haddadi et al., 2006]; see Table AI.

All patients underwent simultaneous EEG-fMRI acquisitions. In 24-patients no IED was captured during the experiment and therefore are not considered further. Data were lost for five patients.

Since we are primarily interested in deviations of the IED-related haemodynamic response from the canonical shape, which is a representation of the response to individual brief stimuli, we have limited our analysis to acquisitions in which IED could be identified individually. Therefore, we have excluded all experiments ($N = 8$) in which the IED of interest occurred in the form of runs, best modeled

as blocks [Salek-Haddadi et al., 2006]. For the same reason, a further three experiments were excluded in which 1,000 IED or more were detected using an automated spike detection method [Salek-Haddadi et al., 2006], leaving 26 acquisitions in 24 patients. In four of those acquisitions, independent right- and left-sided IED were captured and modeled separately, resulting in a total of 30 experiments.

In all patients, the seizure focus was first classified by an investigator who was blind to the fMRI analysis on the basis of the clinical, EEG, video-EEG telemetry, and structural MRI as being localized (one lobe), lateralized (one hemisphere), diffuse or uncertain; see Table I for a summary of the per-fMRI EEG and electro-clinical findings.

Data Acquisition

Acquisition methods have been reported elsewhere [Salek-Haddadi et al., 2006]. Briefly, using MR-compatible equipment, 10 EEG channels (using the 10–20 system) were recorded at Fp1/Fp2, F7/F8, T3/T4, T5/T6, O1/O2, Fz (ground) and Pz as the reference, and bipolar electrocardiogram [Krakow et al., 2000]. Seven hundred and four T2*-weighted single-shot gradient-echo echo-planar images (EPI; TE/TR 40/3,000, flip angle: 90°, 21 interleaved 5 mm thick slices, FOV $= 24 \times 24$ cm^2, 64^2 matrix) were acquired continuously over 35 min on a 1.5 Tesla Horizon Echo-Speed MRI scanner (General Electric, Milwaukee). In cases no. 1, 2, and 5, the acquisition consisted of 450, 600, and 420 scans, respectively. Patients were asked to rest with their eyes shut and to keep their head still.

Cardiac and gradient-related artifacts in the EEG were removed online [Allen et al., 1998, 2000].

EEG Analysis and Event Identification

Online EEG was used to monitor epileptiform activity, head motion, and eye movements. EEG analysis was carried out offline by two expert observers. Each IED was marked manually using a mouse-driven time cursor to create a software-generated list of onsets from the slice-timing information, as captured alongside the EEG for the gradient artifact removal process [Allen et al., 2000].

FMRI Analysis

The aim of the analysis was to identify regions of activation corresponding to noncanonical responses (i.e., not captured by the HRF+TD model) and to compare their location to the regions of activation captured by the HRF+TD model [Salek-Haddadi et al., 2006].

All fMRI data were analyzed using the SPM2 (Statistical Parametric Mapping) software package [http://www.fil.ion.ucl.ac.uk/spm/] and Matlab® version 6.5 R13 (The Mathworks). Images were slice-time corrected, realigned, and spatially smoothed using an isotropic Gaussian kernel of 8 mm Full Width Half Maximum (FWHM).

For each case, a General Linear Model was constructed that was made up of three sets of regressors:

1. Fourier set: Regressors were obtained by convolving a time series of IED time markers with 8 cosines and sines over a 32 s time-window starting at the event onsets [Josephs et al., 1997]. The cosines and sines are modulated by a Hanning window. The assumption underlying this model is that the haemodynamic response can be modeled as the output from a linear low-pass system when an impulse is used as input [Aguirre et al., 1998; Glover, 1999; Lange and Zeger, 1997; Logothetis et al., 2001]. Note that the fact that IED occur randomly relative to scan timing, and given the internal representation of the regressors in the SPM software (16 points per TR), means that the IED-related response is effectively sampled at a higher rate than TR, depending on the number of IED captured [Josephs et al., 1997]. Consequently, there is no risk of over-paramerization by the Fourier basis set;
2. HRF+TD set: EEG event onsets were convolved with the canonical HRF and its temporal derivative (TD) [Salek-Haddadi et al., 2006];
3. Confounds set: Effects of motion were modeled by including 24 realignment parameters and scan-nulling regressors for large (>0.2 mm) motion events [Lemieux et al., 1997; Salek-Haddadi et al., 2003, 2006].

An example of a resulting design matrix is shown in Figure 1.

For each case, a statistical parametric map was obtained to identify 'noncanonical' IED-related responses (i.e., not captured by the HRF+TD model) by performing an F-test across the Fourier basis-set regressors. A significance level of $P < 0.05$ was used, Family-Wise Error corrected based on Gaussian Random Field Theory [Friston et al., 1991]. No cluster threshold was applied and the results are presented as Statistical Parametric Maps (SPMs), using the glass-brain format to allow visualization of the entire activation pattern.

Classification and concordance of activation patterns

Noncanonical responses were plotted for each activated cluster in the form of the fitted response at the cluster statistical maximum and classified visually as either: oscillatory, activation (entirely or mostly positive over the 32 s window), or deactivation (entirely or mostly negative). Oscillatory responses were stereotypical, with 5–6 cycles across the 32 s time window (see Results, Fig. 1).

Where possible, we made categorical judgments regarding the fMRI concordance with the independently determined focus, as described previously [Salek-Haddadi et al., 2006]. Activation patterns were classified as either

TABLE I. EEG data and fMRI results

	Description of IEDs			fMRI						
					Map concordance				Global maximum cluster (Fourier component)	
Experiment	Localization	IED count	Clinical localization (focus)	No of clusters: localization (Fourier component)	C	C+	D	Ø	Time course	No of voxels
1	L-T IED	45	Uncertain	4: L-Post-T, WM (2), R-T		◆	●		Osc	1
2	R IED	82	R-Lat	NULL		●		◆	—	—
5	Frequent Bil synch IED	122	Diffuse	NULL				◆	—	—
6	L-T IED	483	L-Cent/T	4: L-Par, Mid/R-Front (3)		●	◆		Osc	1
8	L-T IED	178	L-Lat	28: L-Post-T/Occ, Bil-Occ, Bil-F		◆			Deact	70
	R-T IED	12		NULL				◆	—	—
9	L-T IED	404	L-T	NULL				◆	—	—
10	Bil SW	59	L-Lat	8: R-Par, Mid-Par, Bil-F			◆		Deact	6
11	L Post-T IED	230	L-Lat	NULL				◆	—	—
12	L Ant-T IED	638	L-T	14: R-T, Occ, L-T		●	◆		Deact	15
15	L Post-T/Occ IED	12	L-Occ/T	NULL				◆	—	—
17	L-T IED	38	L-Lat	NULL				◆	—	—
19	L-lat IED	103	Uncertain	NULL				◆	—	—
21	R-lat IED	73	R-F	NULL				◆	—	—
22	R Ant-T IED	28	Diffuse	2: Cereb, L-T	●		◆		Osc	1
25a	L-F/T IED + L-T IED	630	L-T	1: Pre-Cun		●	◆		Osc	1
26	R-lat IED	27	Uncertain	NULL				◆	—	—
	L-lat IED	30		NULL				◆	—	—
27a	R-T IED	37	R-Lat	NULL		●		◆	—	—
27b	R-T IED	12		NULL				◆	—	—
30	L-lat IED	30	L-Lat	2: R-F			◆	●	Osc	1
31	R-Cent IED + R-Cent slow	447	R-F/Par	NULL	●			◆	—	—
35	L-F/T IED	112	L-Lat	2: R-F, WM	●		◆		Osc	1
36	L-Cent IED	477	L-Par	NULL				◆	—	—
37	L-T IED	72	T (uncertain laterality)	NULL		●		◆	—	—
38a	L-lat IED	11	Diffuse	NULL				◆	—	—
	R-lat IED	36		1: L-F			◆	●	Osc	2
	L-lat IED	26		NULL				◆	—	—
38b	R-lat IED	31		NULL				◆	—	—
39	L-F/T IED	622	L-T	30: Mid-F, L-T, L-Cereb, Occ, Cereb, R-T		●	◆		Act	932

Description of EEG, electroclinical, and fMRI findings for all experiments. Multiple experiments for a given subject are designated by the case number followed by an experiment-specific letter. IEDs described are those captured during the fMRI experiment. Clinical localization gives focus localization based on electroclinical data when possible. Diamonds (◆) indicate concordance for the Fourier component F test (Fourier+HRF+TD+motion model); in cases where degree of concordance differed from that revealed by the HRF+TD F test-derived activation (HRF+TD+motion model), a line joins the two results (HRF+TD result – disk: ●). IED, Interictal epileptiform discharge. Localization: T, temporal; Par, parietal; Occ, occipital; F, frontal; Cereb, cerebellum; R, right; L, left; Bil, bilateral; Mid, midline; WM, white matter; Lat, lateralized; Cent, central; Synch, synchronous; Concordance: C, Concordant; C+, Concordant Plus; D, Discordant; Ø, NULL. Time course: Osc, oscillatory; Act, activation; Deact, deactivation.

Concordant (C), where the entire activation was in the same lobe as the electro-clinical localization; Concordant plus (C+), where the cluster containing the most significant voxel (global maximum) was concordant but additional clusters were seen remote from the presumed focus; Discordant (D), no concordant significant responses; Null (Ø), no significant activation. When the focus was classified as uncertain or diffuse, fMRI concordance was assessed in relation to the presumed generator of the IED. The concordance results for the noncanonical responses were compared with those obtained for the HRF+TD model [Salek-Haddadi et al., 2006].

RESULTS

The experimental data, including the number of IED and their morphology, the HRF+TD and Fourier F-test results are given in Table I. In two experiments, the IED were of a generalized, bilateral nature (no. 5, 10); in the remainder of cases, the discharges were focal or unilateral. The focus localization was diffuse or uncertain in six patients, and lateralized or localized within a lobe in the remainder of cases.

Significant noncanonical responses were revealed in 11/30 experiments (11/24 patients). In four cases, the maps consisted of a single voxel and in the remainder the number of clusters varied between 2 and 30. Nine noncanonical activation patterns were classified as Discordant and the remaining two were classified as Concordant plus.

The visual classification of event-related responses was unambiguous in all cases; at the global maxima, seven responses were classified as Oscillatory, three as Deactivation and one as Activation.

Comparison of Yield and Concordance With HRF+TD Model

Significant responses were revealed in 13/30 experiments (13/24 patients) using the HRF+TD model; three were classified as Concordant, eight Concordant plus, and two as Discordant (see Table I).

In nine experiments, significant responses were revealed using both models and 15 experiments had no significant activation using either model. Overall, the degree of concordance was the same for both models in 16/30 experiments. The most common difference in degree of concordance between the two models was Concordant plus (HRF+TD model) vs. Discordant (Fourier component; four cases), followed by Concordant plus (HRF+TD model) vs. NULL (Fourier; three cases), Concordant (HRF+TD) vs. Discordant (Fourier; two cases), and NULL (HRF+TD) vs. Discordant (Fourier; two cases).

Illustrative Cases

The following cases were selected as follows to be representative of all the results: all cases with nonoscillatory responses, plus two cases with single-voxel clusters and oscillatory responses: one in which the HRF+TD model revealed a significant activation (case no. 1) and one in which it did not (case no. 30).

To facilitate interpretation of the responses in relation to their shape, the results of positive and negative HRF *t* tests (SPM{t}) are illustrated for the HRF+TD model, although significance and concordance (as shown in Table I) were established based on F tests. The SPM canonical HRF is overlaid on the noncanonical time course plots to help illustrate their variability.

Case no. 1 (Fig. 1)

A patient with a previous left anterior temporal lobe resection with frequent, predominantly left temporal IED. The Fourier-derived map was classified as Concordant plus and consisted of four single-voxel clusters. The response at the maximum cluster (left posterior temporal) was classified as oscillatory, as were the responses in the other three significant clusters, which were remote from the presumed IED generator. The HRF+TD map showed deactivation in the right frontal, right parietal, and left frontal lobes and was classified as Discordant.

Case no. 8 (Fig. 2)

A patient with post-traumatic epilepsy of left hemisphere origin. Hundred and seventy-eight left-temporal spikes were recorded during the EEG-fMRI acquisition, which gave rise to significant Blood Oxygen Level-Dependent (BOLD) activation. There was no significant response associated with 12 right-sided discharges. The Fourier-derived map consisted of 28 clusters and was classified as Concordant plus, as was the HRF+TD result. The Fourier set global maximum was located in the posterior part of the left temporal lobe, with additional clusters in the left frontal, right anterior temporal mid-frontal, and occipital lobes. The time course of response at the global maximum was classified as deactivation: the initial part of the curve is slightly positive, followed by 15 s of negative signal change. Interestingly, the response at the second most significant cluster (left inferior frontal) resembled the canonical shape, with an early and narrow peak.

The HRF+TD map showed a BOLD activation extending over the left temporal lobe, with a global maximum located in the anterior part of the lobe. Comparison of the Fourier and HRF+TD results shows that the Fourier global maximum was located at the posterior edge of the main canonical activation. Other noncanonical responses were located either on the edges of the canonical activation or contralateral to it.

Case no. 10 (Fig. 3)

A patient with left hippocampal sclerosis, a history of early febrile convulsions at 11 months, and blank spells

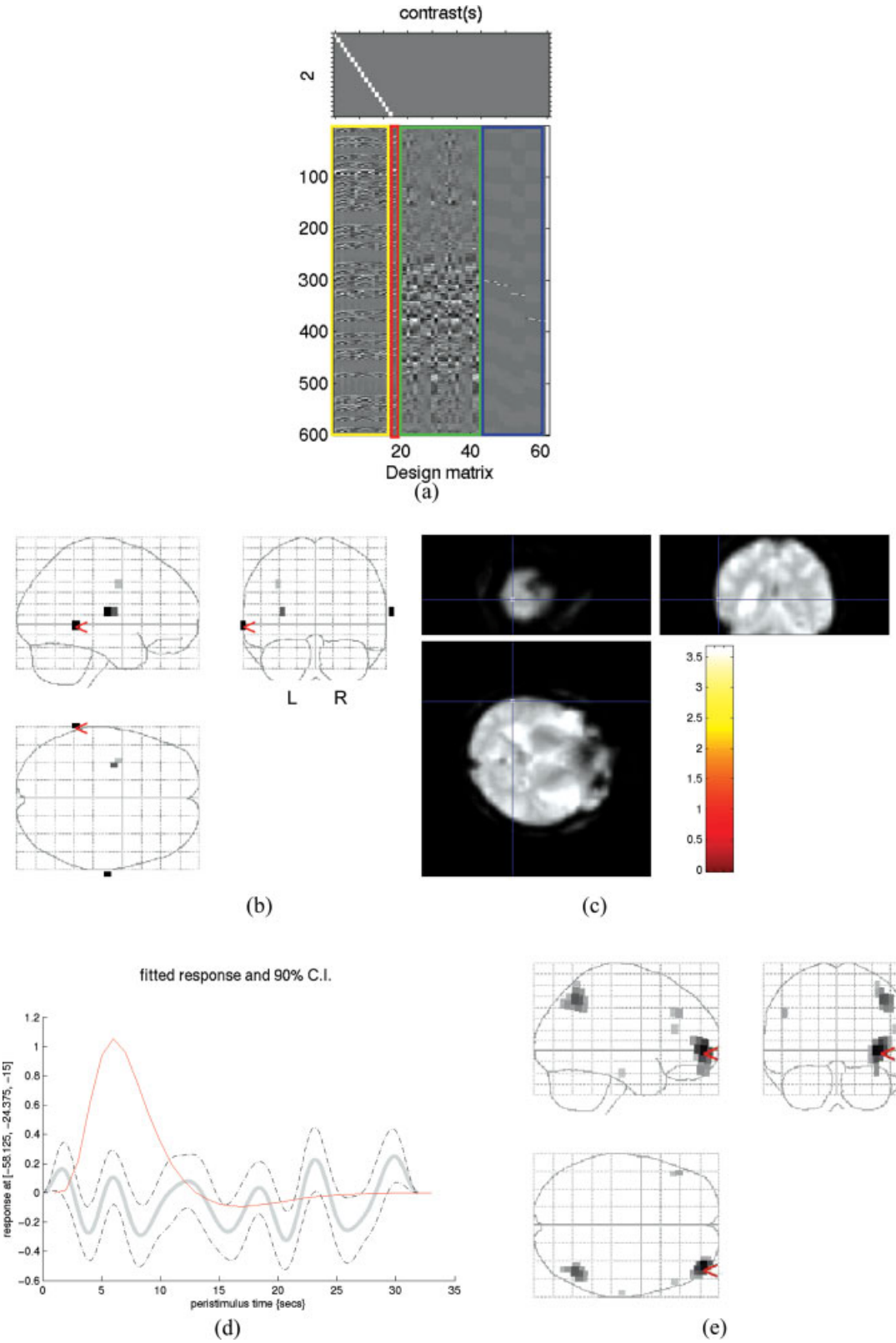
contrast(s)
2
100
200
300
400
500
600
20
40
60
Design matrix
(a)
L
R
(b)
3.5
3
2.5
2
1.5
1
0.5
0
(c)
fitted response and 90% C.I.
response at [-58.125, -24.375, -15]
peristimulus time {secs}
(d)
(e)

Figure 1.

from the age of 3 years, which later developed into complex partial seizures. Bilaterally synchronous bursts of spike-wave discharges were captured during EEG-fMRI. The Fourier-derived map showed a diffuse pattern with a global maximum in the right parietal region with additional clusters in the parietal (midline) and frontal lobes (bilateral), including orbital frontal. The morphology of the responses in the parietal region was biphasic with an initial peak at around 4 s post IED followed by a negative change with a duration of ~12 s. In contrast, the supraorbital response was clearly noncanonical.

The HRF+TD model revealed large areas of activation, mostly posterior and central, and a diffuse deactivation pattern. Comparison of the Fourier and HRF+TD results shows the former to be broadly on the periphery of the canonical activation.

Case no. 12 (Fig. 4)

A patient with left hippocampus sclerosis and left anterior temporal spikes and sharp waves on the EEG. The Fourier-derived map showed a global maximum contralateral to the presumed focus with a negative response. The next two most significant clusters corresponded to mostly negative responses at locations remote from the presumed focus. The HRF+TD model revealed a global maximum in the left-temporal lobe with a positive response and additional, mostly remote, clusters with negative responses.

Case no. 30 (Fig. 5)

A patient with normal structural MRI and left lateralized IED (spikes, sharp waves, and slow-waves) were recorded during EEG-fMRI. The Fourier-derived map showed two small clusters contra-lateral to the EEG activity with oscillatory time courses. No significant activation was revealed using the HRF+TD model.

Case no. 39 (Fig. 6)

A patient with left hippocampal sclerosis and frequent left temporal IED. The global maximum for the Fourier model was located in the fronto-orbital region with a noncanonical, positive, response. The second (left temporal lobe), third (cerebellum), and fourth (parieto-occipital) most significant clusters had similar noncanonical, positive, responses. For the HRF+TD model, the activation was limited to the posterior part of the brain, where it was similar to the Fourier-derived pattern though less extensive, with global maximum in the left temporal region. HRF+TD deactivation was found in the cerebellum and left frontal region.

DISCUSSION

We have investigated the presence of IED-related responses that deviate from the 'canonical' shape and the relationship between noncanonical responses and the presumed generator of the IED in a consecutive series of patients with focal epilepsy. To this end, we used a modeling approach that combines the standard, canonical, response model, and a flexible model based on a Fourier basis set. This allows one to map regions with a significant amount of event-related BOLD signal variance above and beyond that explained by the canonical model using appropriate F contrasts. To simplify the analysis and interpretation and in view of previous findings on nonlinear effects, we focused on isolated IED, excluding runs.

Using this approach we found significant noncanonical responses in roughly 1/3 of experiments. This is slightly lower than the proportion of the same patients in whom significant activation was found using the canonical model. We note that these yields were significantly lower than those reported in previous studies of patients with focal epilepsy, which ranged from 60% to 70% [Al Asmi et al., 2003; Krakow et al., 1999, 2001; Salek-Haddadi et al., 2006]. This difference can be explained by the exclusion from the present study of runs of spikes, which tend to be associated with more significant BOLD changes [Salek-Haddadi et al., 2006].

The time-course of the responses captured by the Fourier model varied; some resembled the canonical one but others were characterized by sustained positive or sustained negative responses. The noncanonical responses tended to be remote from the presumed focus or IED generator, as reflected in the much lower degree of concordance for the Fourier-derived responses compared with the standard model. Noncanonical response maps were classified as being Concordant plus in only two cases, including one consisting of single voxel clusters with oscillatory response shapes. The remainder of cases with significant noncanonical responses was classified as Discordant.

Figure 1.

Case no. 1. (**a**) Illustration of design matrix showing the nested model. Fourier basis set regressors are outlined in yellow; HRF+TD regressors outlined in red; 24 motion (scan realignment) parameters outlined in green; 'scan-nulling' regressors outlined in blue; (**b**) SPM{F} of Fourier basis set regressors overlaid onto glass brain—the global maximum is indicated in red; (**c**) overlay of activation pattern onto mean EPI image—crosshair at global maximum; (**d**) time course (fitted response) of IED-related fMRI signal at global maximum—vertical axis shows % signal change relative to baseline, with canonical HRF (peak amplitude normalised to unity) shown in red; (**e**) SPM{T} for HRF+TD model overlaid onto glass brain +HRF contrast (taken from web material in Salek-Haddadi et al., [2006]). [Color figure can be viewed in the online issue, which is available at www.interscience.wiley.com.]

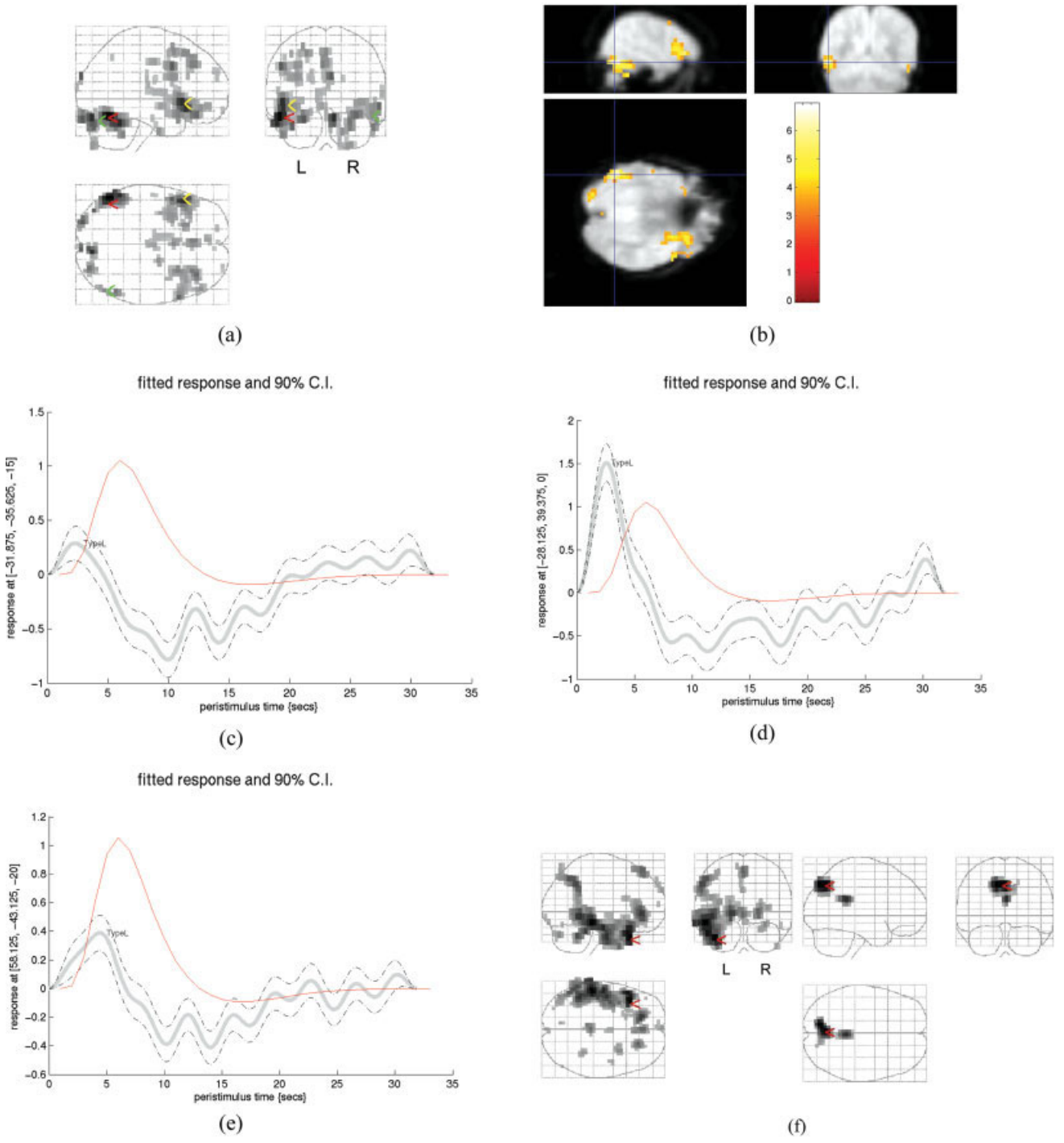

Figure 2.

Case no. 8. (**a**) SPM{F} of Fourier basis set regressors overlaid onto glass brain—the global maximum is indicated in red, the cluster containing the second most significant voxel is indicated in yellow and the one containing the third most significant cluster in green; (**b**) overlay of activation pattern onto mean EPI image—crosshair at global maximum; (**c**) time course (fitted response) of IED-related fMRI signal at global maximum—vertical axis shows % signal change relative to baseline, with canonical HRF shown in red; (**d**) time course (fitted response) of IED-related fMRI signal at second most significant voxel; (**e**) time course (fitted response) of IED-related fMRI signal at third most significant voxel; (**f**) SPM{T} for HRF+TD model overlaid onto glass brain: left shows +HRF contrast, right shows −HRF contrast (taken from web material in Salek-Haddadi et al., [2006]). [Color figure can be viewed in the online issue, which is available at www.interscience.wiley.com.]

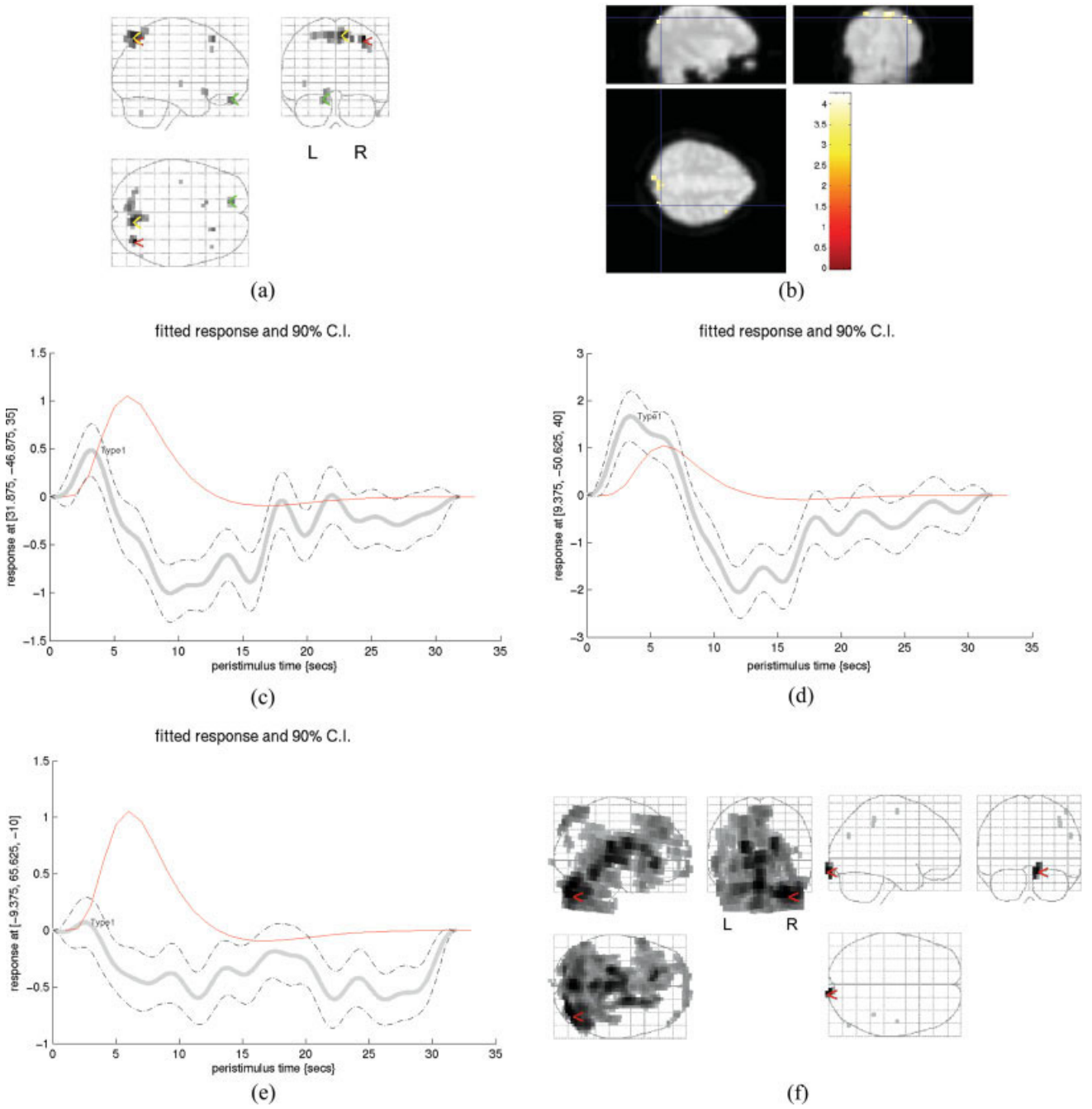

Figure 3.

Case no. 10. (**a**) SPM{F} of Fourier basis set regressors overlaid onto glass brain—the global maximum is indicated in red, the cluster containing the second most significant voxel is indicated in yellow and the one containing the third most significant cluster in green; (**b**) overlay of activation pattern onto mean EPI image—crosshair at global maximum; (**c**) time course (fitted response) of IED-related fMRI signal at global maximum—vertical axis shows % signal change relative to baseline, with canonical HRF shown in red; (**d**) time course (fitted response) of IED-related fMRI signal at second most significant voxel; (**e**) time course (fitted response) of IED-related fMRI signal at third most significant voxel; (**f**) SPM{T} for HRF+TD model overlaid onto glass brain: left shows +HRF contrast, right shows −HRF contrast (taken from web material in Salek-Haddadi et al., [2006]). [Color figure can be viewed in the online issue, which is available at www.interscience.wiley.com.]

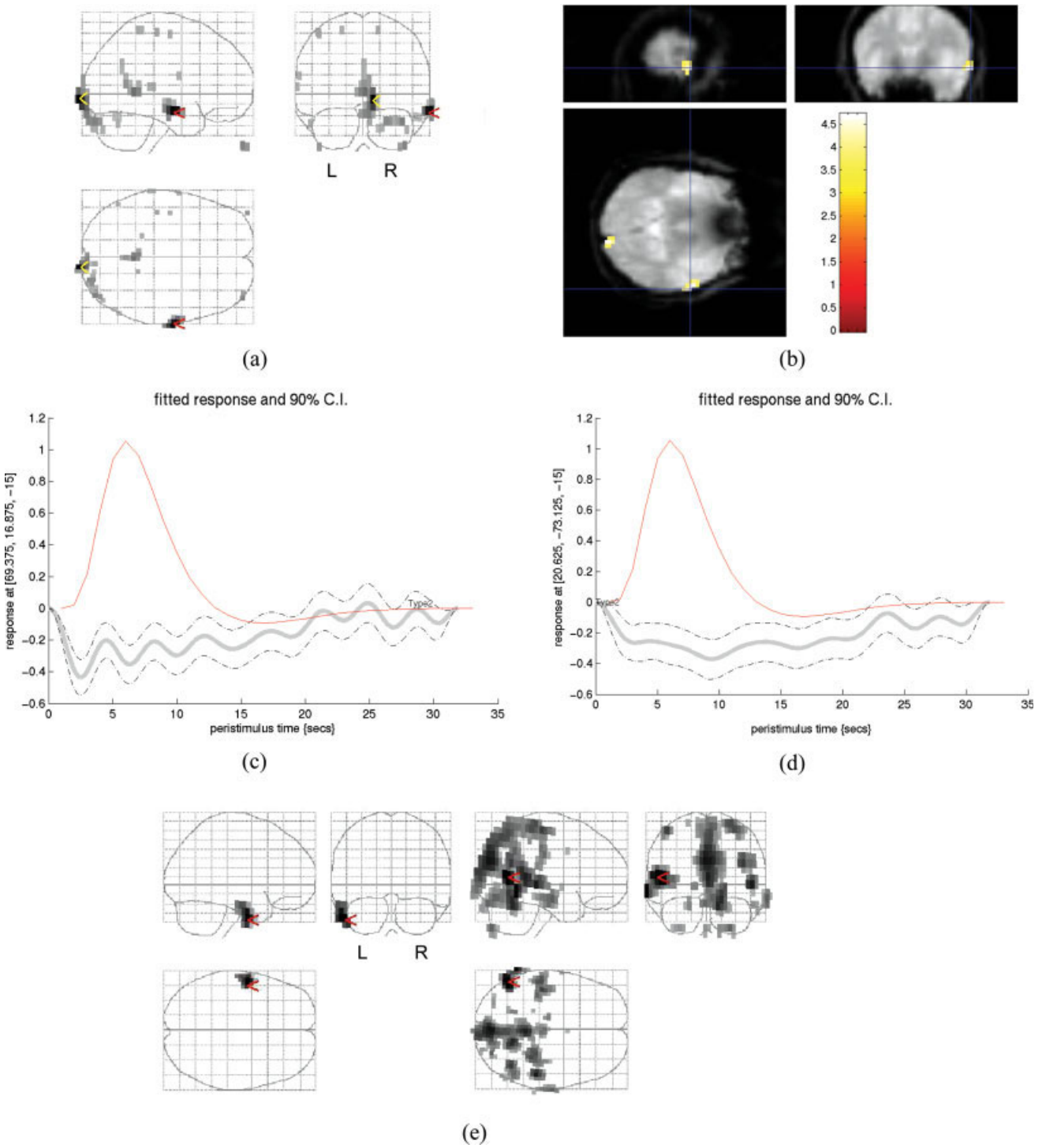

Figure 4.

Case no. 12. (**a**) SPM{F} of Fourier basis set regressors overlaid onto glass brain—the global maximum is indicated in red and that containing the second most significant voxel is indicated in yellow; (**b**) overlay of activation pattern onto mean EPI image—crosshair at global maximum; (**c**) time course (fitted response) of IED-related fMRI signal at global maximum—vertical axis shows % signal change relative to baseline, with canonical HRF shown in red; (**d**) time course (fitted response) of IED-related fMRI signal at second most significant voxel; (**e**) SPM{T} for HRF+TD model overlaid onto glass brain: left shows +HRF contrast, right shows −HRF contrast (taken from web material in Salek-Haddadi et al., [2006]). [Color figure can be viewed in the online issue, which is available at www.interscience.wiley.com.]

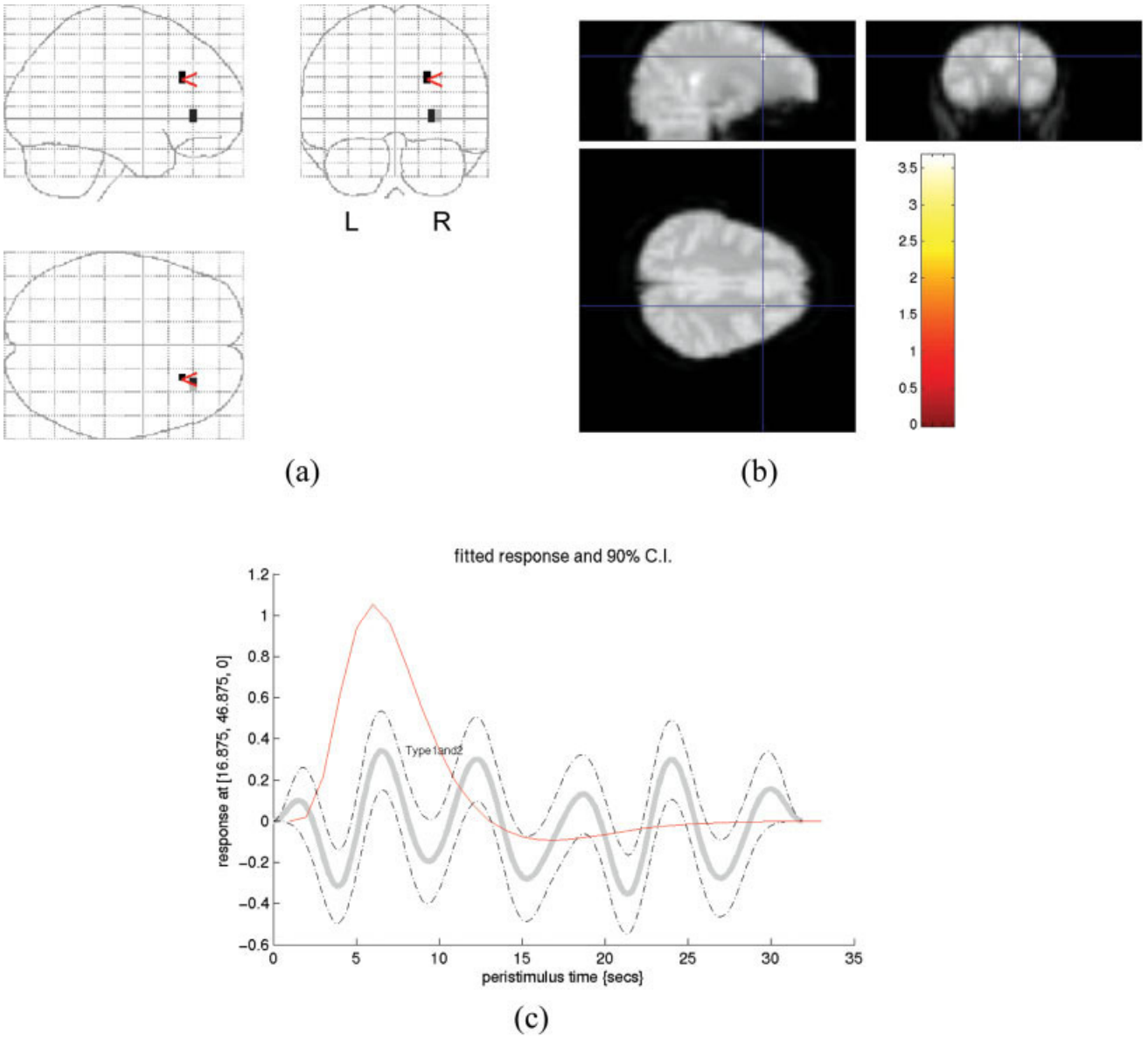

Figure 5.

Case no. 30. (**a**) SPM{F} of Fourier basis set regressors overlaid onto glass brain—the global maximum is indicated in red; (**b**) overlay of activation pattern onto mean EPI image—crosshair at global maximum; (**c**) time course (fitted response) of IED-related fMRI signal at global maximum—vertical axis shows % signal change relative to baseline, with canonical HRF shown in red. [Color figure can be viewed in the online issue, which is available at www.interscience.wiley.com.]

A commonly observed type of noncanonical responses could be termed 'high-frequency' (but in most cases not purely) oscillations. These had widely varying amplitudes in absolute and relative terms, and were generally remote from the presumed generator and usually confined to single-voxel clusters. Each of these characteristics does not necessarily invalidate them however; the overall pattern is suggestive of data over-fitting (noise fitting) in addition to possible false positive activations (controlled at 0.05 on a family-wise basis).

Noncanonical responses classified as deactivations were observed in three experiments and varied in their shape and location in relation to the presumed generators. The following general characteristics emerged: noncanonical responses located in the periphery of the areas of canonical activation or deactivation (cases no. 8, 10, 12); noncanonical responses contra-lateral to the presumed focus (cases no. 8, 12); some responses look like distorted forms of the canonical shape, with amplified undershoots (cases no. 8, 10); some sustained negative, but also positive responses,

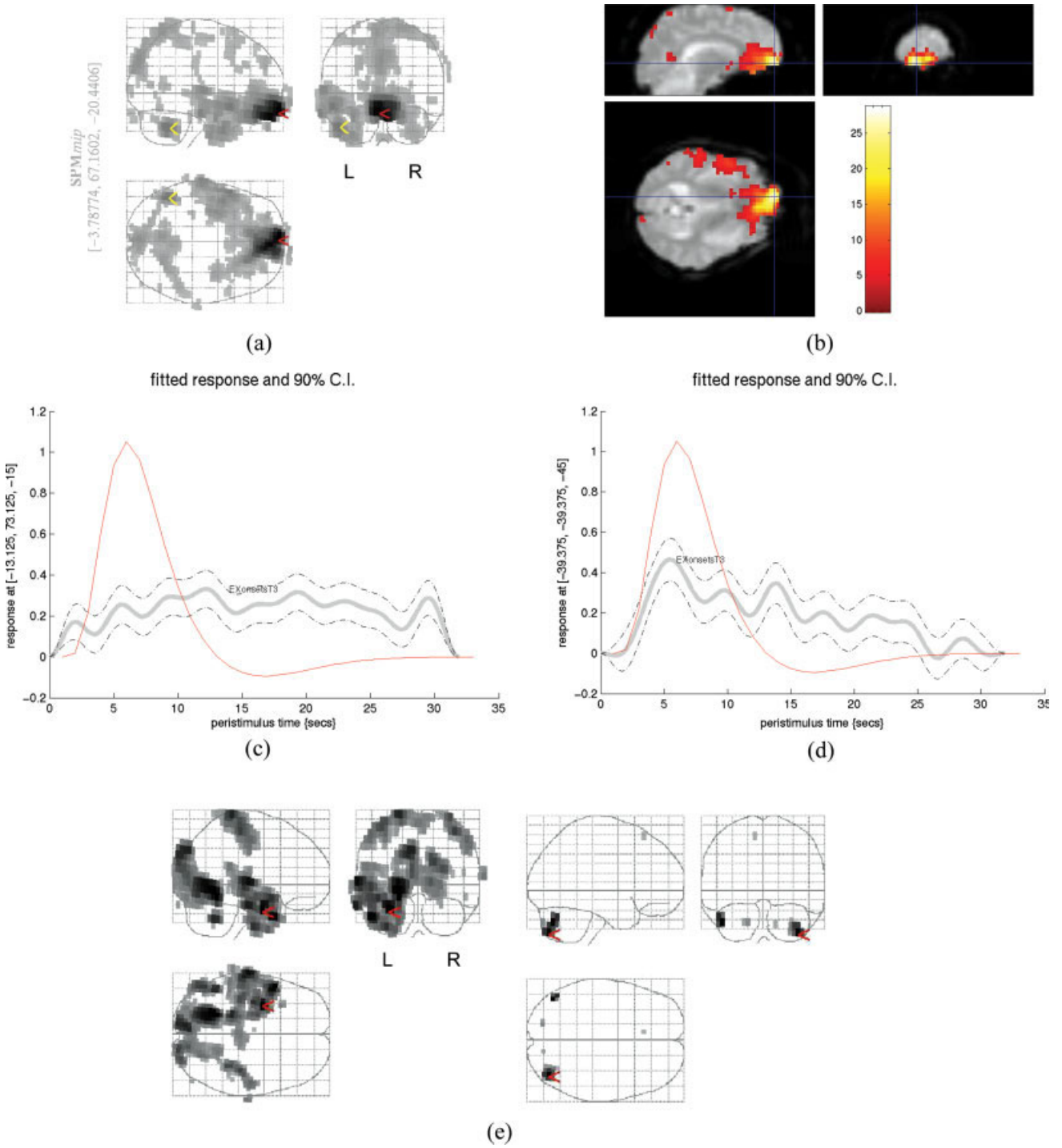

Figure 6.

Case no. 39. (**a**) SPM{F} of Fourier basis set regressors overlaid onto glass brain—the global maximum is indicated in red and that containing the second most significant voxel is indicated in yellow; (**b**) overlay of activation pattern onto mean EPI image—crosshair at global maximum; (**c**) time course (fitted response) of IED-related fMRI signal at global maximum—vertical axis shows % signal change relative to baseline, with canonical HRF shown in red; (**d**) time course (fitted response) of IED-related fMRI signal at second most significant voxel; (**e**) SPM{T} for HRF+TD model overlaid onto glass brain: left shows +HRF contrast, right shows −HRF contrast (taken from web material in Salek-Haddadi et al., [2006]). [Color figure can be viewed in the online issue, which is available at www.interscience.wiley.com.]

in particular in the supra-orbital region and sagittal sinus (cases no. 10, 12). There was a single case in which only positive noncanonical responses were captured (no. 39): these were extensive and covered an area in the periphery of the canonical responses, extending more anteriorly into the supra-orbital region. We also noted that the pattern seems to follow the posterior part of the superior sagittal sinus.

Methodological Aspects

We chose a modeling approach based on a GLM comprising two nested models, allowing the identification of regions for which one model (e.g. Fourier in this instance) explains a significant amount of variance above and beyond the other (e.g., HRF+TD). As in standard fMRI analyses, the significance of the effects thus revealed is a function of the ratio of variance explained by the model over the residual, and therefore can reflect various degrees of deviation from the canonical shape, from small but consistent to larger but less consistent. Nonetheless, all responses corresponding to the Fourier set regressors are labeled noncanonical. The Fourier basis set is only one of a number of similar approaches that can capture inter-regional response shape variability, such as Finite Impulse Response (FIR) and Gamma functions, but we did not seek to compare those methods. It has already been shown that the Fourier basis set can capture IED-related responses in a number of studies [Henson, 2003]; given a sufficiently high order it can capture an arbitrarily shaped response (as for the FIR model) within the constraints that it is null at event onset and resolves to zero at the end of the chosen time window due to the Hanning modulation; it is more efficient at capturing small deviations from the canonical shape than the FIR model [Penny et al., 2006]. A model order of eight was chosen following a preliminary analysis of six randomly selected cases in which we observed a significant proportion of variance explained by the highest order terms.

We chose to assess concordance of the fMRI findings at the whole map level, based on the position of the statistical global maximum and other activation clusters in relation to the position and lobes containing the presumed generator of the IED [Salek-Haddadi et al., 2006]. This approach combined with the presentation of the complete activation pattern is designed to allow the entire findings to be accurately represented in a concise fashion.

The use of F contrasts for the creation of the SPMs reflects the type of response model used, whereby one must test for voxels at which the fitted response may be represented as any linear combination of the chosen basis functions. In this work, we chose to assess the degree of concordance for the two models based on F contrasts as a matter of fairness and simplicity. The use of T contrast images for illustration of the results is designed to facilitate the interpretation of the event-related time courses and to reflect the emerging understanding of fundamental differences between positive (generally in the proximity of the presumed focus) and negative (generally remote) IED-related BOLD changes.

Biological Significance

The basic assumption that underlies the conventional modeling approach for IED-correlated fMRI is that the haemodynamic correlate of individual spikes resembles that of a brief external stimulus that elicits a normal (canonical) response. The fact that this approach has been successful for identifying regions of activation in numerous studies and in particular with a good degree of spatial concordance in cases with a clearly identified focus supports this assumption [Krakow et al., 1999, 2001; Salek-Haddadi et al., 2006]. The findings of this study suggest that similar mechanisms link both normal brain activity and individual IED (spikes) to the haemodynamic response.

It seems a priori unlikely that regions remote from the focus showing noncanonical responses sustain brain activity or neurophysiological mechanisms that are more abnormal (pathological) than those within or near the focus. Assuming our assessment of the focus localization to be accurate and indicative of all pathology (when possible) in the present series, this suggests that noncanonical responses may reflect factors other than local epileptogenicity. Confirmation of this hypothesis will require further investigation based on the comparison of BOLD and invasive EEG investigation.

These considerations raise the issue of the nature of the observed noncanonical responses. A priori, these may reflect one or a combination of the following phenomena: physiological noise (cardiac, respiration); signal changes from large vessels; unusually fast signal changes; residual motion-related signal change; mismatch between scalp EEG and underlying activity; abnormal neurovascular coupling; propagation of the epileptiform activity to regions remote from the primary generator.

Physiological noise, namely signal fluctuations linked to cardiac and respiratory activity, is an important problem in fMRI [Lund et al., 2006]. Although respiration-related noise is concentrated in the edges of the brain, in the ventricles, and around the main vessels and cardiac noise tends to be concentrated in the brainstem and in the immediate vicinity of large vessels, these are present throughout the brain. In our data, the period of the oscillatory responses was of the order of 4 s, corresponding to the lower limit of the Fourier set used here. This frequency is in the range of flow or pulsation artifacts. We also note the presence of such oscillations superimposed onto slower components (10–20 s) for all Fourier-derived time courses found here.

It is known that large task-/event-related signal changes can occur in large vessels leading to a contamination of BOLD maps [Lai et al., 1993; Menon et al., 1993; Segebarth et al., 1994], and that these venous changes are slower [De

Martino et al., 2006]. In our data, we have observed sustained (positive) responses in regions known to harbor large vessels, such as the superior sagittal sinus.

Although motion-related signal changes were modeled thoroughly in this work, there remains a risk of residual motion and stimulus-correlated signal change. In two cases we observed noncanonical responses in the supra-orbital region, with monophasic time courses lasting 20–30 s. This region is known to be particularly sensitive to motion due to strong susceptibility gradients associated with sinuses. Therefore, these may represent false activation due to the large signal variations that may coincide with epileptiform activity on a small number of occasions.

Propagation of IED can give rise to two effects: excitation and increased inhibition at remote locations. Furthermore, propagation is a stochastic process, modulated by prior history and local state. Therefore, fluctuations in the time-locked BOLD signal at distant propagation sites, when averaged across events, could result in weak and noisy responses. Furthermore, it has also been shown that the IED-related deactivation time course can be more delayed than an inverted canonical response [Benar et al., 2002; Salek-Haddadi et al., 2006]. Flexible models may better be able to capture such effects and changes that are weighted sums of variable responses to each spike. In this study, we have observed noncanonical, negative responses in periphery of the area of canonical activation and contralaterally (cases no. 8, 10, 12).

It is well known that IED recorded on scalp EEG generally reflect a small proportion of ongoing epileptiform activity and therefore can introduce an important bias in the analysis of IED-correlated fMRI data [Salek-Haddadi et al., 2003], which would also represent non-BOLD effects such a rapid field perturbations linked to neuronal currents [Liston et al., 2004]. In cases 8 and 10 additional 'early' responses with a shape that resembles the canonical response were revealed, which may also reflect activity that precedes the IED recorded on the scalp and propagation. For example, activity synchronous to the IED used for fMRI modeling may be too weak to be detected directly, leading to BOLD changes remote from the presumed primary generator [Benar et al., 2006]. It is possible that scalp discharges that appear as brief, individual spikes correspond to longer paroxysmal events, which would lead to a mismatch between the canonical model and the actual signal change which could be better detected using a more flexible model. This may explain some of the sustained responses uncovered in this study.

Modelling Implications

The core issue to consider when selecting a modeling strategy in fMRI is the aim of the investigation one wants to achieve, and in particular the hypotheses to be tested. Our results suggest that the conventional, canonical HRF+TD modeling approach is the most likely to provide localizing information on the primary generator of IED. However, in some circumstances including a more flexible basis set in the GLM, such as the Fourier used in this work (or alternative: FIR, Gamma functions), or using deconvolution, may allow additional regions of activation to be revealed albeit at the possible cost of overall sensitivity. This would be important if noncanonical responses were linked to genuine epileptiform activity rather than artifacts or downstream effects.

CONCLUSIONS

Regions of IED-related BOLD changes with time courses that deviate from the canonical shape were detected in a large proportion of cases studied. In all but one case, the noncanonical activations were remote from the presumed primary IED generator. In the majority of cases, their spatiotemporal pattern was suggestive of artifacts. This supports the assertion that the canonical model should be the favored approach for the localization of IED-related BOLD changes, with a potential complementary role for more flexible models in view of further exploring the networks involved in the generation of IED.

ACKNOWLEDGMENTS

The National Society for Epilepsy supports the MRI Unit and JSD. Thanks to Professor Karl Friston (Wellcome Department of Imaging Neuroscience, Institute of Neurology, UCL) for comments on the manuscript and Will Penny, of the same department, for his technical advice.

REFERENCES

Aguirre GK, Zarahn E, D'Esposito M (1998): The variability of human, BOLD hemodynamic responses. NeuroImage 8:360–369.

Al Asmi A, Benar CG, Gross DW, Khani YA, Andermann F, Pike B, Dubeau F, Gotman J (2003): fMRI activation in continuous and spike-triggered EEG-fMRI studies of epileptic spikes. Epilepsia 44:1328–1339.

Allen PJ, Polizzi G, Krakow K, Fish DR, Lemieux L (1998): Identification of EEG events in the MR scanner: The problem of pulse artifact and a method for its subtraction. Neuroimage 8:229–239.

Allen PJ, Josephs O, Turner R (2000): A method for removing imaging artifact from continuous EEG recorded during functional MRI. NeuroImage 12:230–239.

Bagshaw AP, Kobayashi E, Dubeau F, Pike B, Gotman J (2005): Correspondence between EEG-fMRI and EEG dipole localisation of interictal discharges in focal epilepsy. Epilepsia 46:36–36.

Benar CG, Gross DW, Wang Y, Petre V, Pike B, Dubeau F, Gotman J (2002): The BOLD response to interictal epileptiform discharges. NeuroImage 17:1182–1192.

Benar C, Grova C, Kobayashi E, Bagshaw A, Aghakhani Y, Dubeau F, Gotman J (2006): EEG-fMRI of epileptic spikes: Concordance with EEG source localization and intracranial EEG. Neuroimage 30:1161–1170.

De Martino F, Gentile F, Esposito F, Balsi M, Di Salle F, Goebel R, Formisano R (2006): Classification of fMRI independent compo-

nents using IC-fingerprints and support vector machine classifiers. Neuroimage 34:177–194.
Diehl B, Salek-Haddadi A, Fish DR, Lemieux L (2003): Mapping of spikes, slow waves, and motor tasks in a patient with malformation of cortical development using simultaneous EEG and fMRI. Magn Reson Imaging 21:1167–1173.
Friston KJ, Frith CD, Liddle PF, Frackowiak RSJ (1991): Comparing functional (PET) images: The assessment of significant change. J Cereb Blood Flow Metab 11:690–699.
Friston KJ, Frith CD, Turner R, Frackowiak RSJ (1995a): Characterizing evoked hemodynamics with fMRI. NeuroImage 2:157–165.
Friston KJ, Holmes AP, Poline J-B, Grasby PJ, Williams SCR, Frackowiak RSJ, Turner R (1995b): Analysis of fMRI time-series revisited. NeuroImage 2:45–53.
Friston KJ, Fletcher P, Josephs O, Holmes A, Rugg MD, Turner R (1998): Event-related fMRI: Characterizing differential responses. NeuroImage 7:30–40.
Glover GH (1999): Deconvolution of impulse response in event-related BOLD fMRI. NeuroImage 9:416–429.
Hamandi K, Salek-Haddadi A, Fish DR, Lemieux L (2004): EEG/functional MRI in epilepsy: The Queen Square experience. J Clin Neurophysiol 21:241–248.
Handwerker DA, Ollinger JM, D'Esposito M (2004): Variation of BOLD hemodynamic responses across subjects and brain regions and their effects on statistical analyses. NeuroImage 21:1639–1651.
Henson RNA (2003): Analysis of fMRI time series. In: Richard SJF, Karl JF, Christopher DF, Raymond JD, Cathy JP, Semir Z, John A, William P, editors. Human Brain Function. San Diego, Elsevier/Academic Press. p 793–822.
Josephs O, Turner R, Friston KJ (1997): Event-related fMRI. Hum Brain Mapp 5:243–248.
Krakow K, Woermann FG, Symms MR, Allen PJ, Lemieux L, Barker GJ, Duncan JS, Fish DR (1999): EEG-triggered functional MRI of interictal epileptiform activity in patients with partial seizures. Brain 122(Part 9):1679–1688.
Krakow K, Allen PJ, Lemieux L, Symms MR, Fish DR (2000): Methodology: EEG-correlated fMRI. Adv Neurol 83:187–201.
Krakow K, Lemieux L, Messina D, Scott CA, Symms MR, Duncan JS, Fish DR (2001): Spatio-temporal imaging of focal interictal epileptiform activity using EEG-triggered functional MRI. Epileptic Disord 3:67–74.
Lai S, Hopkins AL, Haacke EM, Li D, Wasserman BA, Buckley P, Friedman L, Meltzer H, Hedera P, Friedland R (1993): Identification of vascular structures as a major source of signal contrast in high resolution 2D and 3D functional activation imaging of the motor cortex at 1.5T: Preliminary results. Magn Reson Med 30:387–392.
Lange N, Zeger SL (1997): Non-linear Fourier time series analysis for human brain mapping by functional magnetic resonance imaging. Appl Stat J Roy Stat Soc Ser C 46:1–19.
Lazeyras F, Blanke O, Perrig S, Zimine I, Golay X, Delavelle J, Michel CM, de Tribolet N, Villemure JG, Seeck M (2000): EEG-triggered functional MRI in patients with pharmacoresistant epilepsy. J Magn Reson Imaging 12:177–185.
Lemieux L, Allen PJ, Franconi F, Symms MR, Fish DR (1997): Recording of EEG during fMRI experiments: Patient safety. Magn Reson Med 38:943–952.
Lemieux L, Salek-Haddadi A, Josephs O, Allen P, Toms N, Scott C, Krakow K, Turner R, Fish DR (2001): Event-related fMRI with simultaneous and continuous EEG: Description of the method and initial case report. Neuroimage 14:780–787.
Liston AD, Salek-Haddali A, Kiebel SJ, Hamandi K, Turner R, Lemieux L (2004): The MR detection of neuronal depolarization during 3-Hz spike-and-wave complexes in generalized epilepsy. Magn Reson Imaging 10:1441–1444.
Logothetis NK, Pauls J, Augath M, Trinath T, Oeltermann A (2001): Neurophysiological investigation of the basis of the fMRI signal. Nature 412:150–157.
Lu Y, Bagshaw AP, Grova C, Kobayashi E, Dubeau F, Gotman J (2006): Using voxel-specific hemodynamic response function in EEG-fMRI data analysis. Neuroimage 32:238–247.
Lund TE, Madsen KH, Sidaros K, Luo WL, Nichols TE (2006): Non-white noise in fMRI: Does modelling have an impact? Neuroimage 29:54–66.
Menon RS, Ogawa S, Tank DW, Ugurbil K (1993): Tesla gradient recalled echo characteristics of photic stimulation-induced signal changes in the human primary visual cortex. Magn Reson Med 30:380–386.
Patel MR, Blum A, Pearlman JD, Yousuf N, Ives JR, Saeteng S, Schomer DL, Edelman RR (1999): Echo-planar functional MR imaging of epilepsy with concurrent EEG monitoring. Am J Neuroradiol 20:1916–1919.
Penny W, Flandin G, and Trujillo-Barreto N (2006): Bayesian comparison of spatially regularised general linear models. Human Brain Mapp(in press).
Rajapakse JC, Kruggel F, Maisog JM, andvon Cramon DY (1998):: Modeling hemodynamic response for analysis of functional MRI time-series. Human Brain Mapping 6, 283–300.
Salek-Haddadi A, Friston KJ, Lemieux L, Fish DR (2003): Studying spontaneous EEG activity with fMRI. Brain Res Rev 43:110–133.
Salek-Haddadi A, Diehl B, Hamandi K, Merschhemke M, Liston A, Friston K, Duncan JS, Fish DR, Lemieux L (2006): Hemodynamic correlates of epileptiform discharges: An EEG-fMRI study of 63 patients with focal epilepsy. Brain Res 1088:148–166.
Seeck M, Lazeyras F, Michel CM, Blanke O, Gericke CA, Ives JR, Delavelle J, Golay X, Haenggeli CA, de Tribolet N, Landis T (1998): Non-invasive epileptic focus localization using EEG-triggered functional MRI and electromagnetic tomography. Electroencephalogr Clin Neurophysiol 106:508–512.
Segebarth C, Belle V, Delon C, Massarelli R, Decety J, Le Bas JF, Decorps M, Benabid AL (1994): Functional MRI of the human brain: predominance of signals from extracerebral veins. Neuroreport 5:813–816.
Warach S, Ives JR, Schlaug G, Patel MR, Darby DG, Thangaraj V, Edelman RR, Schomer DL (1996): EEG-triggered echo-planar functional MRI in epilepsy. Neurology 47:89–93.
Zou P, Mulhern RK, Butler RW, Li CS, Langston JW, Ogg RJ (2005): BOLD responses to visual stimulation in survivors of childhood cancer. NeuroImage 24:61–69.

TABLE AI. Electroclinical data

Case	Onset age (y)	Aetiology	Seizure type	Structural MRI	Ictal EEG	Interictal EEG
1	0	Post left temporal lobectomy for DNET, plus R-HS	CPS, SGTCS	Extensive left temporal lobectomy with considerable amount of altered brain surrounding cavity.	Subdural electrodes: LEFT frontal or possibly contralateral seizure onset, outside of the resected areas	Intermittent and widespread theta. Frequent temporal sharp waves and spikes with shifting lateralization, predominantly left mid temporal.
2	7	MCD	FMS	Diffuse cortical thickening right hemisphere, within parietal and occipital lobes, extending to frontal region.	Right temporal spikes	Widespread, right-sided spikes, sharp waves, and sharp and slow waves maximal frontocentral and centrotemporally.
5	0	MCD	CPS, SGTCS	Extensive MCD involving both hemispheres.	—	Left-sided spikes, sharp waves and slow waves, some bilaterally synchronous and occasionally right-sided.
6	40	Chronic encephalitis	FMS, CPS, SGTCS	Mild atrophy of left cerebral hemisphere.	Widespread over left hemisphere	Left midtemporal spikes and slow waves.
8	5	Post-traumatic	SGTCS	MRI negative	—	Left temporal slowing with frequent left anterior temporal spikes.
9	1	L-HS	SPS, CPS.	Severe diffuse L-HS	No lateralization	Left anterior temporal spikes.
10	4	L-HS	CPS, SGTCS	L-HS	Left lateralization	Bursts of left-sided frontotemporal spikes. Sometimes occurring bilaterally.
11	0	Perinatal subarachnoid haemorrhage	CPS, SGTCS	Left cystic encephalomalacia plus L-HS	—	Left-sided slowing with left posterior temporal spikes.
12	1	Unknown (Family history, post-vaccine seizures, and L-HS)	MJ, SPS, CPS, SGTCS	L-HS	No lateralization	Left anterior temporal spikes and sharp waves.
15	5	Cryptogenic occipital lobe epilepsy	SPS (Visual phenomena R≫L)	MRI negative	—	Left posterior temporal/occipital spikes and sharp waves.
17	3	Grade II left parietal astrocytoma resected at age 11	SPS, SGTCS	Large temporoparietal resection.	Widespread over left hemisphere	Left posterior temporo-parietal spikes.
19	7	Cryptogenic	CPS (extra-temporal semiology), SGTCS	MRI negative	Bilateral onset	Left temporal sharp waves and spikes with bilateral frontal sharp waves.
21	4	MCD	SPS, FMS, SGTCS.	Right parietal open leptoschizencephaly.	—	Bursts of spike-wave activity over central region bilaterally.
22	5	DNET	SPS, SGTCS	Right temporal lobe lesion involving amygdale and uncus but not hippocampus.	No clear lateralization[a]	Right-sided anterior temporal spikes with some independent left-sided spikes.
25	1	Neoplasm	CPS, SGTCS	Mass in left temporal lobe involving amygdala, hippocampus and parahippocampal gyrus associated with irregular cystic cavity.	No clear change	Left anterior temporal spikes.
26	4	FCD	CPS, SGTCS	Focal signal change in left middle frontal gyrus consistent with focal cortical dysplasia.	—	Independent left and right mid-temporal spikes and slow-waves. L≫R.
27	7	MCD	CPS, SGTCS	Marked malformation affecting both hemispheres, mainly the right. The right hemisphere is smaller and the fronto parietal regions are most affected.	—	Spikes, sharp-waves, and slow-waves widespread over the right.
30	8	Cryptogenic	CPS, SGTCS	MRI negative	Widespread over left hemisphere	L fronto-temporal bursts of spikes, sharp waves, and spike and slow-waves.
31	0	MCD	SPS, CPS, SGTCS	Two large heterotopic nodules: frontoparietocentral and medial parietal.	—	Frequent right centro-parietal spikes.

TABLE AI. (continued)

Case	Onsetage (y)	Aetiology	Seizure type	Structural MRI	Ictal EEG	Interictal EEG
35	<10	MCD	SPS, CPS, SGTCS	Left hemisphere atrophy with parietal polymicrogyria and L-HS.	Widespread over left hemisphere	Left anterior-mid temporal spikes.
36	3	FCD	SPS	Thickened cortex in the left antero-inferior parietal region just extending into the inferior frontal gyrus.	No change	Continuous Left parietal spikes.
37	14	L-HS	CPS (temporal semiology)	Severe diffuse L-HS.	Independent right and left seizure onsets with temporal lobe-type automatisms. Psychometry non-lateralizing.	Left anterior-mid temporal spikes and slow waves.
38	5	Cryptogenic	CPS, SGTCS	MRI negative	—	Right-sided mid-anterior temporal sharp waves plus rare independent left-sided sharp waves.
39	7	L-HS	CPS, SGTCS	L-HS	Left temporal onset	Left anterior temporal spikes.

[a] No. 22: Two distinct seizure types were recorded during video telemetry. One type would begin with a peculiar feeling around the head, followed by head slumping to the right, unresponsiveness and post-ictal dysphasia lasting minutes. Here, ictal changes were seen bilaterally but greater on the left. The second type began with the same aura followed by clasping together of the hands, rocking movements of the arms, followed by fidgeting and secondary generalisation into a tonic-clonic seizure. This attack began with right fronto-temporal fast activity.